



Title	Can attenuated total internal reflection-fourier transform infrared be used to understand the interaction between polymers and water? A hyperspectral imaging study
Authors(s)	Mukherjee, Sindhuraj, Martínez-González, J. A., Stallard, Charlie P., Dowling, Denis P., Gowen, Aoife
Publication date	2017-04-07
Publication information	Mukherjee, Sindhuraj, J. A. Martínez-González, Charlie P. Stallard, Denis P. Dowling, and Aoife Gowen. "Can Attenuated Total Internal Reflection-Fourier Transform Infrared Be Used to Understand the Interaction between Polymers and Water? A Hyperspectral Imaging Study." IM Publications Open, April 7, 2017. https://doi.org/10.1255/jsi.2017.a3 .
Publisher	IM Publications Open
Item record/more information	http://hdl.handle.net/10197/11356
Publisher's version (DOI)	10.1255/jsi.2017.a3

Downloaded 2026-05-01 23:37:41

The UCD community has made this article openly available. Please share how this access benefits you. Your story matters! (@ucd_oa)



© Some rights reserved. For more information

1 **CAN ATR-FTIR BE USED TO UNDERSTAND THE INTERACTION**
2 **BETWEEN POLYMERS AND WATER?**
3 **A HYPERSPECTRAL IMAGING STUDY.**

4 **S. Mukherjee¹, J. A. Martínez-González¹, C. P. Stallard², D. P. Dowling², A. A. Gowen¹**

5 ¹*School of Biosystems and Food Engineering, University College Dublin, Belfield, Dublin 4, Ireland.*

6 ²*School of Mechanical and Materials Engineering, University College Dublin, Belfield, Dublin 4, Ireland.*

7 Keywords: ATR-FTIR, polymer, HMDSO, hydrophobicity, silicon, water, Hyperspectral Imaging, wetting

8 **ABSTRACT**

9 This study investigates the potential use of Attenuated Total Internal Reflection – Fourier
10 Transfer Infrared (ATR-FTIR) imaging, a hyperspectral imaging modality, to investigate
11 molecular level trends in the interaction of water with polymeric surfaces of varying
12 hydrophobicity. The hydrophobicity of two categories of polymeric biomaterials is
13 characterised using contact angle (CA) measurements and their relationship with the band area
14 of the OH stretching $\bar{\nu}_s$ vibration of water over time is presented. This is supported with
15 correlations between CA data and single wavenumber intensity values (univariate analysis).
16 Multivariate analysis of the spectra captured at the OH stretch for all polymers is carried out
17 using Principal Component Analysis (PCA) to study the spatial variation in the interaction
18 between the polymeric surfaces and water. Finally, a comparison between the univariate and
19 multivariate strategies is presented to understand the interaction between polymeric
20 biomaterials and water.

21 **INTRODUCTION**

22 Polymeric biomaterials are widely used in different applications for example, in packaging¹,
23 pharmaceuticals², medical devices and implants³. The surface properties of such polymeric
24 biomaterials influence phenomena such as permeability, hydrophilicity⁴, diffusion, protein

25 adsorption⁵, biocompatibility and degradation⁶. These phenomena are also affected by the
26 nature of the interaction between such polymeric biomaterials and water. For example, Tanaka
27 et al.⁷, hypothesised that specific water layers at the proximity of biomedical polymers such
28 as poly(ethylene glycol), polyvinylpyrrolidone, poly(methylvinylether), in contact with blood
29 determine the biocompatibility of these polymers by influencing the conformation of
30 subsequently adsorbed proteins to allow certain moieties to bond with the surface while
31 exposing others to water for hydrogen bonding. Chen et al.⁸, discussed the importance of
32 surface hydration in biofouling and found that highly hydrated surfaces generally exhibit non-
33 fouling behaviour. Chandler⁹ and Bunkin et al.¹⁰, have reported differences in water structure
34 near hydrophobic moieties, but the nature of the interaction is not very well understood. It has
35 been proposed that this interaction is conditioned by the formation of hydrogen bonds between
36 the surface of the polymeric biomaterial and water⁹. In order to understand the behaviour and
37 operational limitations of polymeric biomaterials in biological systems that are largely
38 composed of water, it is desirable to understand this interaction further¹¹.

39 In this work, ATR-FTIR imaging was investigated to study the interaction between water and
40 polymeric biomaterials with a wide range of hydrophobicity. The aim of the study was to
41 investigate correlations between contact angle measurements with ATR-IR imaging
42 spectroscopic measurements of wetted polymers.

43 **MATERIALS & METHODS**

44 **Polymer samples and HMDSO coated silicon samples**

45 Three commercial test samples of polymers PTFE, PET (MylarTM) and UHMPE were obtained
46 from CS Hyde Company (1351 N. Milwaukee Avenue, Lake Villa, Illinois, USA), and
47 characterised for hydrophobicity. From this point onwards in the manuscript, these commercial
48 polymers samples are referred to as “bulk polymers”.

49 Hexamethydisiloxane (HMDSO) coatings were polymerised using a modified plasma
 50 enhanced chemical vapour deposition technique developed at UCD's School of Mechanical
 51 and Materials Engineering, as described in more detail in a previous paper¹². Films were
 52 deposited onto silicon wafers, resistivity 0-100 M Ω .cm (450 μ m thick) supplied by PI-KEM
 53 Ltd. using an atmospheric pressure plasma jet. Prior to film deposition the wafers were
 54 ultrasonically cleaned in methanol, followed by acetone and propanol, air dried and pre-treated
 55 with He/O₂ plasma. The films were deposited from HMDSO (Aldrich \geq 99.5 %) using
 56 deposition conditions aimed at forming films with a range of water contact angles. The
 57 deposition conditions used to deposit hydrophilic, hydrophobic and superhydrophobic films
 58 has previously been carried out with a system explained in a different article⁵. Deposition
 59 conditions used in this study are given in Table 1.

60 **Table 1:** Deposition conditions and measured contact angle of plasma polymerised HMDSO films.

HMDSO film	Monomer flow rate (μ lmin ⁻¹)	Plasma Gas Composition	Measured contact angle (24 h, after deposition).
Hydrophilic	25	He, N ₂ , O ₂	5
Hydrophobic	25	He, N ₂	105
Superhydrophobic	5	He, N ₂	150

61 Gas flow rates He: 5 slm, N₂: 0.70 slm, O₂: 0.25 slm. Plasma discharge power: 7.5 W

62 All samples were stored in sealed petri dishes at room temperature for up to 4 months (bulk polymers)
 63 and 6 months (HMDSO coated wafers). For each polymer group studied, the same sample was tested
 64 at each time point.

65 **Contact Angle Measurements**

66 The hydrophobic effect of each material surface was quantified via water contact angle (CA)
 67 measurements, using the sessile drop technique¹³. This technique measures the level of
 68 hydrophobicity of a material surface based on the balance of interfacial free energies presented
 69 by a three phase boundary system when the liquid comes in contact with a solid surface under

70 ambient conditions¹⁴. Water contact angle measurements were recorded at three separate
71 spatial locations in the central region of each sample using a DataphysicsTM OCA-20
72 goniometry system under room conditions.

73 The hydrophobic behaviour of HMDSO coated wafers over the time was studied by comparing
74 a control set (kept in a sealed box at room conditions) and an experimental set (hydrated and
75 used to collect experimental data). Bulk polymers behaviour was assumed to be stable at room
76 conditions.

77 The HMDSO monomer was used to deposit nanometre thick coatings with a range of wetting
78 properties. In the case of each coating, the monomer chemistry used was the same.
79 Modification of hydrophobicity was achieved by altering deposition process conditions to
80 slightly alter either the surface chemistry or surface roughness of the coatings. This warranted
81 its own investigation, whereas, the bulk polymers' hydrophobicity is based on chemical
82 differences and probably roughness too.

83 **ATR-FTIR scan acquisition**

84 A Thermo ScientificTM NicoletTM iNTM10 Infrared Microscope (10× magnification, Mercury-
85 Cadmium-Tellurium (MCT) detector, working range 7800–650 cm⁻¹ with a 4 cm⁻¹ spectral
86 resolution) was used with a germanium crystal (refractive index = 4) to collect all Attenuated
87 Total Internal Reflection – Fourier Transfer Infrared (ATR-FTIR) spectra. This system is fitted
88 with two types of detector, a point detector, which collects spectra pixel by pixel and an array
89 detector, which collects spectra over a collection of points or pixels, before moving onto the
90 next spatial location resulting in a higher speed of collection. Initially the array detector was
91 used to collect hyperspectral images, however, after the 2nd month of data collection, we found
92 that the array detector presented noise in the spectral collection which was difficult to remove.
93 Therefore, we decided to use the point detector for the rest of the spectral collection (i.e. months

94 3 - 6). Additionally, spectral data from the 3rd month of the HMDSO wafers dataset had to be
95 removed due to a problem with the analysis of the superhydrophobic sample.

96 All spectra collected were combined in a data matrix called a 'data cube' where each pixel of
97 the data cube contains a specific spectrum from the polymeric biomaterial. The pixel sizes for
98 data cubes captured by the point detector and array detector were $100\ \mu\text{m} \times 100\ \mu\text{m}$ and $25\ \mu\text{m}$
99 $\times 25\ \mu\text{m}$. The data cubes captured using the array detectors had a step size of $375\ \mu\text{m} \times 75\ \mu\text{m}$,
100 whereas the data cubes captured with the point detector had a step size of $100\ \mu\text{m} \times 100\ \mu\text{m}$.
101 This arrangement gave various sized areas captured by the two detectors. The number of
102 spectra at month 1 was 130 for PET (13*10), 91 for PTFE (13*7) and 169 for UHMPE (13*13).
103 For month 2, 793 spectra (13*61) were collected for each polymer and for subsequent months
104 100 spectra (10*10) were obtained for each polymer. The images extracted from data cubes
105 were scaled to the same size by using the autoscaling option in the Matlab figure properties
106 editor to provide a visual comparison between the differently sized images.

107 ATR spectra of the dry and wetted polymers were obtained. Wetted polymer spectra were
108 captured after hydrating the polymers at room temperature with an equilibration time of at least
109 30 minutes by trapping water using Blu TackTM to construct a well on the surface. Deionised
110 (DI) water was used to wet the polymers, sourced from a Thermo ScientificTM BarnsteadTM
111 Smart2PureTM water purification system (water Type I ASTM, resistance is $18.2\text{M}\ \Omega\cdot\text{cm}$ at
112 temperature 25.6°C).

113 **Data analysis**

114 Water shows two characteristic spectral features in the mid-infrared, i.e., the OH bending
115 vibration, $\bar{\nu}_B$, around 1640cm^{-1} and the OH stretching vibration, $\bar{\nu}_S$, between $3800\text{-}3000\text{cm}^{-1}$
116 ^{15,16}. Both bands could serve as candidates to study how the interaction between biomaterials
117 and water affect the formation of hydrogen bonds. We selected the OH $\bar{\nu}_S$ band because some

118 rotational-vibrational polymer bands appear at the same region as the OH $\bar{\nu}_B$ vibration band
119 (shown in **Figure 1**). Also, Tassaing *et al.* found that greater changes occur in the OH $\bar{\nu}_S$ region
120 as compared to the OH $\bar{\nu}_B$ region when analysing the mid IR spectra of supercritical water at
121 different pressures¹⁷, suggesting that the OH $\bar{\nu}_S$ region is more sensitive to hydrogen bonding
122 between water molecules.

123 The imaging spectra of two categories of polymeric biomaterials tested, i.e., bulk polymers and
124 HMDSO coated wafers, were concatenated separately into two different larger data matrices,
125 one for bulk polymers and other for HMDSO coatings. The spectra for each polymer was
126 extracted from these normalised cubes and averaged to obtain a mean spectrum for each
127 material sample. The matrices were further subsetted to extract the OH $\bar{\nu}_S$ region and subjected
128 to standard normal variate normalisation or SNV¹⁸ in order to minimise spectral variations
129 arising from morphology of the samples.

130 The Pearson correlation coefficient¹⁹ between the intensity of SNV treated mean spectra of the
131 OH $\bar{\nu}_S$ region and the mean value of the contact angle was calculated to study the relationship
132 between the OH $\bar{\nu}_S$ region and the hydrophobicity. The significance of the correlation
133 coefficients was determined by calculating the probability value (p-value) for accepting or
134 rejecting the null hypothesis at a 5% level of significance. The null hypothesis here refers to
135 no correlation between the two variables; intensity of SNV treated mean spectra at a specific
136 wavenumber of the OH $\bar{\nu}_S$ region and the mean value of the contact angle.

137 The wavenumber within the OH $\bar{\nu}_S$ vibration region showing the highest Pearson correlation
138 coefficient was selected and the spatial variation in wetting of the polymeric surfaces at this
139 particular wavenumber was visualised. The experimental OH $\bar{\nu}_S$ band is a combination of the
140 symmetric and asymmetric stretch; and changes in the hydrophobicity of the polymeric
141 biomaterial could be related with change in the intensity or position of the bands. Therefore,

142 the band area of the OH $\bar{\nu}_S$ region was also extracted from the SNV treated mean spectra and
143 compared to the contact angle to further investigate the response of the IR spectra of the wetted
144 surfaces to changes in hydrophobicity.

145 Principal Component Analysis (PCA)²⁰ was carried out to visualize variation in the ATR-IR
146 imaging spectra of the wetted biomaterials studied. The OH $\bar{\nu}_S$ region was extracted from the
147 data matrix containing combined imaging spectra for each category of polymeric biomaterial
148 and subjected to SNV treatment. Then PCA was applied, and the variance explained by each
149 principal component (PC) was calculated. Each PC is a summary of the variation in a dataset
150 and is independent of other PCs. Score images of relevant PCs were analysed to visualise the
151 spatial variation. The Pearson correlation coefficient between the average PC score values and
152 contact angle of the polymeric biomaterials was also calculated to identify the most highly
153 correlated PC with the contact angle measurement. Lastly, the score values of this PC were
154 plotted as a function of the contact angle of the polymeric biomaterials and compared against
155 the band area of the OH $\bar{\nu}_S$ region.

156 The contact angle data were analysed using Origin 9.0 (OriginLab ®, Northampton, MA) and
157 all spectral treatment and analysis was carried out using Matlab (Matlab 2014b, The
158 MathWorks Inc., Natick, MA, 2000).

159 **RESULTS & DISCUSSION**

160 **Contact Angle Measurements**

161 The CA data of the bulk polymers (**Table 2**) indicate their hydrophobic nature as well
162 differences in measured hydrophobicity at different spatial locations.

163 According to the contact angle data collected, the hydrophobicity of the bulk polymers
164 increased in this order: Mylar (PET), UHMPE and PTFE, consistently at all time points.

165 **Table 2** CA data (mean value and standard deviation in degree) for the bulk polymers over 4 months stored in the
166 laboratory (standard conditions).

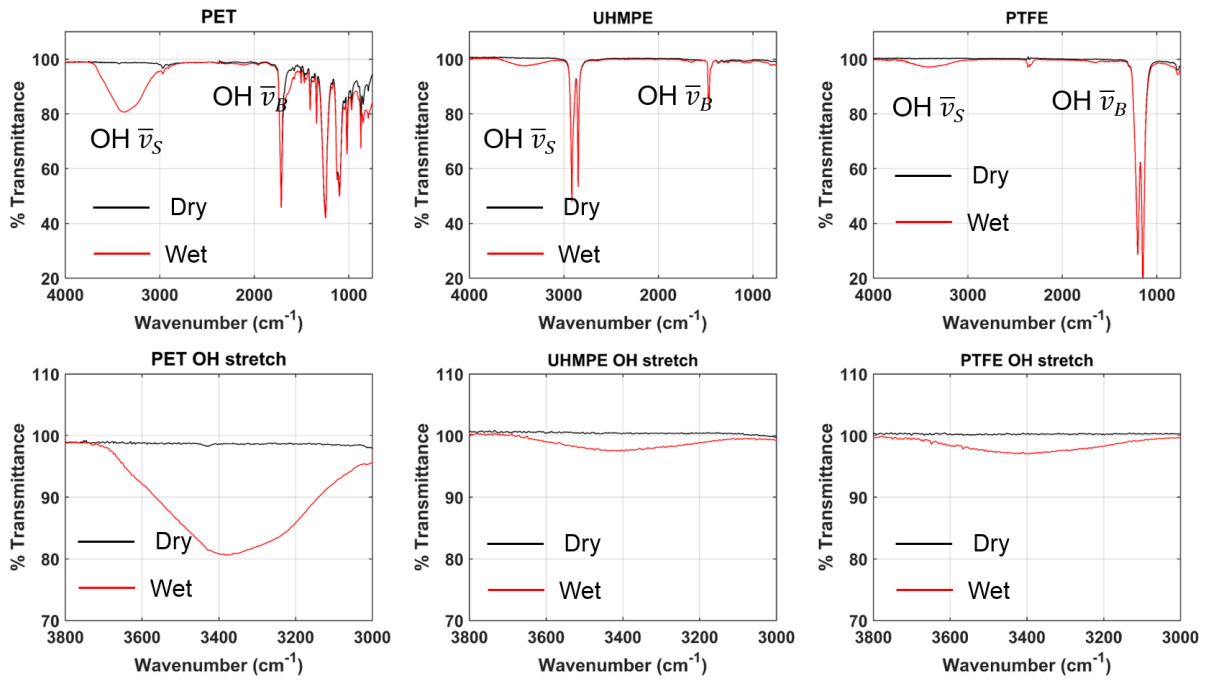
	Month 1	Month 2	Month 3	Month 4
PET	86.95 ± 12.75	66.58 ± 9.83	72.69 ± 0.44	77.59 ± 2.31
UHMPE	87.91 ± 1.85	94.76 ± 4.58	95.53 ± 4.61	83.35 ± 2.48
PTFE	109.74 ± 9.97	131.12 ± 6.61	150.61 ± 3.81	128.87 ± 12.58

167

168 Some differences in spatial variation of the contact angle were noted. Variations in CA data
169 measurements are expected at the different spatial locations over time, since CA data collected
170 at first location for month 1 is not the same as first location for rest of the months for each
171 polymer. It should also be noted that it is necessary to keep the surface totally flat when the
172 CA measurement is obtained. The effect of fixing the sample at different positions to obtain a
173 surface as flat as possible could explain the dispersion of the CA values for PET at month 1.
174 Finally, the protocol applied to collect CA and ATR-FIR measurements, repeated hydration
175 and crystal pressure, may have affected the surface properties.

176 **ATR-FTIR results**

177 The dry and wetted averaged spectra of the bulk polymers collected for the first month are
178 presented in **Figure 1**. Spectral features of PET, UHMPE and PTFE are seen at 2000-1000 cm⁻¹
179 ¹, 3000-2500 cm⁻¹, and 1500-1000 cm⁻¹ respectively. Spectral features of water, i.e., the OH $\bar{\nu}_S$
180 region (3800-3000 cm⁻¹) and OH bending band $\bar{\nu}_B$ (1640 cm⁻¹) are also visible in the wet
181 spectra of the bulk polymers. As mentioned before, the OH $\bar{\nu}_S$ region, which is free from any
182 overlap, was chosen for the analysis because the OH bend $\bar{\nu}_B$ overlaps with one of the native
183 spectral feature of PET, (shown in **Figure 1**, upper section).



184

185 **Figure 1.** Raw dry (black line) and wet (red line) mean spectra from bulk polymers collected from the 1st month.

186 Lower section focusses on the OH $\bar{\nu}_S$ region which is free from overlapping native polymer bands.

187 Non pre-treated wet pixel spectra of the bulk polymers present great variations in the OH $\bar{\nu}_S$

188 region. **Figure 2** shows this spectral variation for the entire spectral range as well as the OH

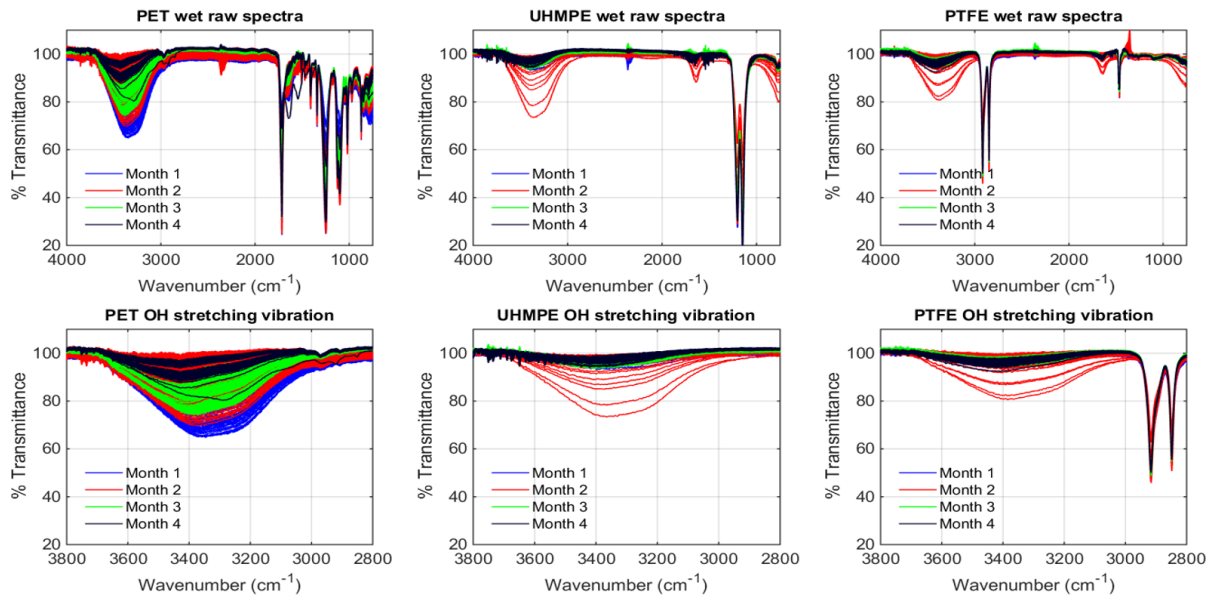
189 $\bar{\nu}_S$ region. Such spectral variations are commonly encountered due to variations resulting from

190 the array detector and sample morphology inherent to the bulk polymers. The OH $\bar{\nu}_S$ region

191 spectra were normalised with SNV to reduce this spectral variation. The results of this pre-

192 treatment are compared with the raw spectra in **Figure 3**.

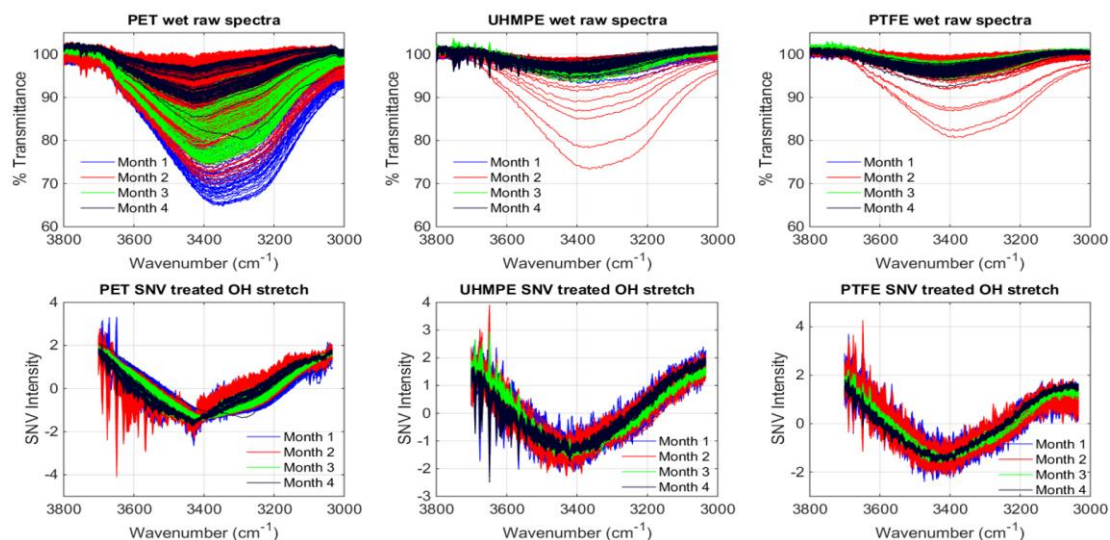
193



194

195 **Figure 2.** Raw (untreated) spectra of bulk polymers at all time points. Lower section focusses on the OH $\bar{\nu}_s$ region
 196 of wet spectra. Intense spectral variation is seen for Mylar (PET) – month 1.

197 The untreated or the wet raw spectra of the bulk polymers from all time points are presented in
 198 the upper section of **Figure 3**. The y-axis has been scaled so that the reader can visualise the
 199 spectral variation which was reduced on the application of the pre-treatment. The lower section
 200 shows the wet SNV treated spectra for the bulk polymers. While the spectral variation is
 201 reduced, the spectra collected for Month 1 and Month 2 show some noise in their spectral
 202 features. This is mostly likely due to the noise attributed to the array detector which was used
 203 to collect data for the first two months.



204

205 **Figure 3.** Effect of SNV normalisation on the OH $\bar{\nu}_s$ region for PET (right), UHMPE (centre) and PTFE (left)
 206 along the time. The top portion of the figure shows the untreated spectra, whereas the bottom portion shows the
 207 effect of the pre-treatment.

208 More hydrophobic polymers minimise water from spreading their surface⁹. Previously, the
 209 level of water absorption on a polyethylene glycol based pharmaceutical polymer²¹ has been
 210 studied using the band area of the OH stretch. As part of this study we wanted to determine if
 211 this metric provides a good approximation to visualise the repulsion of water by the bulk
 212 polymers. The mean band area of the OH $\bar{\nu}_s$ over the four time points is presented in **Table 3**.

213 **Table 3** Values of the mean and standard deviation for the band area $\bar{\nu}_s$ region for the bulk polymers over time.
 214 The values are provided for comparison with Figure 3.

	Month 1	Month 2	Month 3	Month 4
PET	6635 ± 3471.64	2611.72 ± 1905.29	7211.81 ± 1691.57	3092.28 ± 1076.54
UHMPE	738.13 ± 118.63	895.57 ± 441.48	1531.17 ± 252.94	1512 ± 263.96
PTFE	960 ± 324.268	1041.32 ± 457.07	1869.53 ± 241.31	1625 ± 225.81

215

216 PET presented the largest variation in the band area for all months, as observed in **Table 3**.

217 These variations could be compared with the CA data in Table 2. In both cases the variation

218 was maximum for the first two months. For the two other polymers, UHMPE and PTFE, similar
219 changes in the OH $\bar{\nu}_s$ band area have been found. The data from **Table 2** and **Table 3** suggests
220 that there could exist correlations between the band area of the wavenumbers of the OH stretch
221 region and the contact angle data. If any correlation exists, then the specific wavenumber (s)
222 could be used to understand the interaction between polymeric biomaterials and water. The
223 Pearson correlation coefficient was calculated between the band area of the SNV treated mean
224 spectra of the OH stretch for the bulk polymers and the CA data, and a low correlation
225 coefficient value of -0.34 was found. This seemed to indicate that a weak decorrelation between
226 the OH stretch band area and the CA data exists, i.e., as the contact angle (i.e., hydrophobicity)
227 increases, the OH stretch band area increases. However, this required further investigation
228 because the OH stretch represents almost 300 wavenumber variables and is composed of
229 symmetric and asymmetric components. Therefore, the Pearson correlation coefficient
230 between the intensity of the SNV treated mean spectra of each wavenumber of the stretching
231 vibration and CA data for each polymer was presented in **Figure 4**.

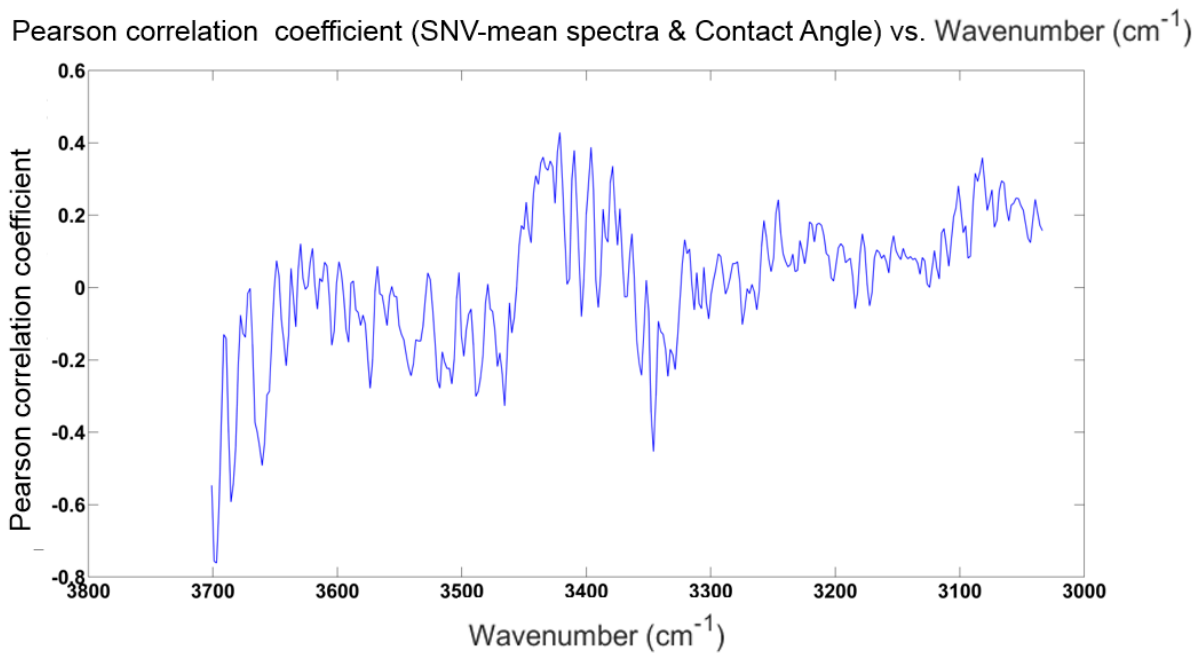


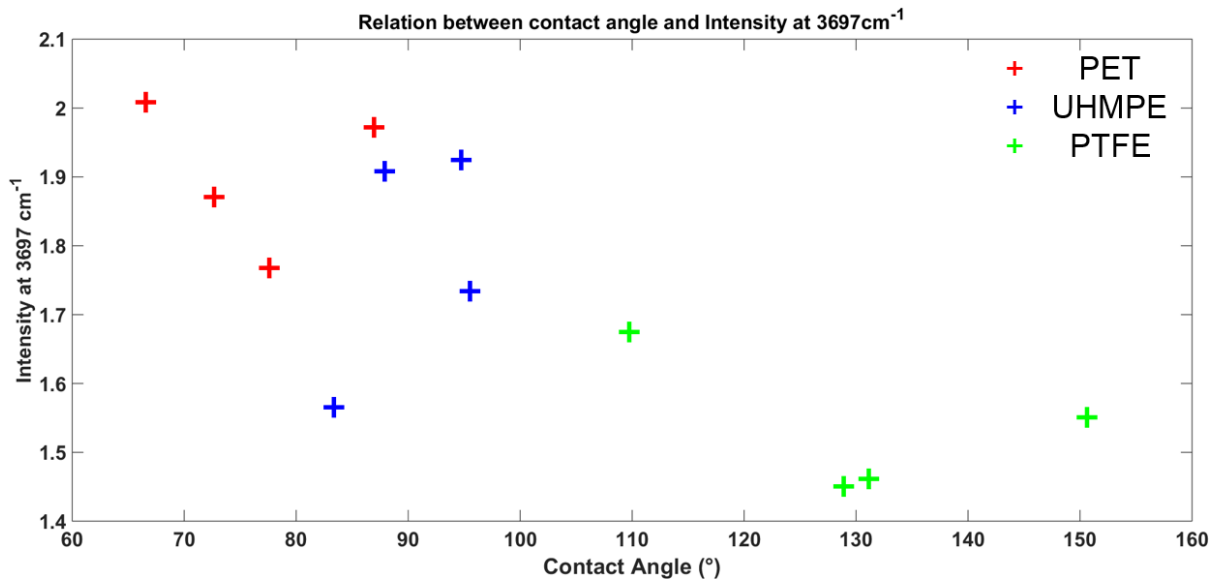
Figure 4. Pearson correlation coefficient between the intensity of the SNV treated mean spectra of each

234 wavenumber of the stretching vibration and CA data of each polymer. Wavenumber at 3697 cm⁻¹ shows a
235 relatively high correlation coefficient (-0.76).

236 The results show that the highest negative correlation between the wavenumbers of the
237 stretching vibration and CA was found at 3697 cm⁻¹ with a value of -0.76 (p-value = 0.0040).
238 The significance of this correlation coefficient was determined by calculating the probability
239 value (p-value) at a 5% level of significance. The null hypothesis here refers to no correlation
240 between the two variables (i.e. intensity of SNV treated mean spectra of the OH $\bar{\nu}_S$ region and
241 the mean value of the contact angle of the bulk polymers). Since the p-value (0.0040) at 3697
242 cm⁻¹ is less than the 5% significance level (p=0.05), we accept our alternate hypothesis, i.e.,
243 the correlation coefficient at this wavenumber is significant.

244 In previous studies on metallic oxides (Al₂O₃ and TiO₂) and lipid membranes 3697 cm⁻¹ was
245 associated with the presence of dangling²² or disturbed²³ hydrogen bonds as a response to the
246 hydrophobicity of the surface. It is reasonable to assume that a hydrophobic surface would
247 disturb hydrogen bonding between the surface and water, which is what our correlation analysis
248 indicates, i.e., as the CA of the surface increases, the intensity of the feature at 3697 cm⁻¹
249 becomes less (shown in **Figure 5**). The weakness of the correlation, however, should be pointed
250 out. This may be related to noise in the SNV treated ATR-IR spectra, as previously mentioned.
251 Following this study the spatial variation of the interaction between water and bulk polymers
252 was analysed at 3697 cm⁻¹.

253

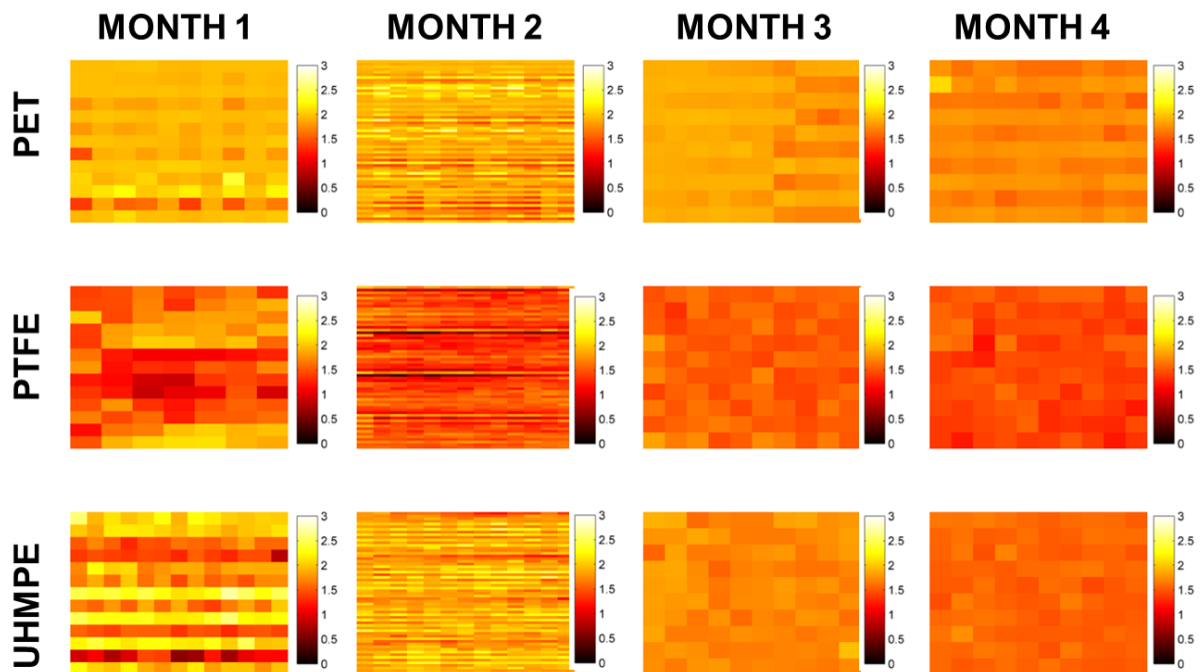


254

255 **Figure 5.** Absorption intensity at 3697 cm⁻¹ (feature showing maximum correlation) plotted as a function of

256 contact angle.

Spatial Variation at 3697cm⁻¹



257

258 **Figure 6.** Spatial variation of % of transmittance intensity at 3697 cm⁻¹ for PET (up), UHMPE (centre) and PTFE

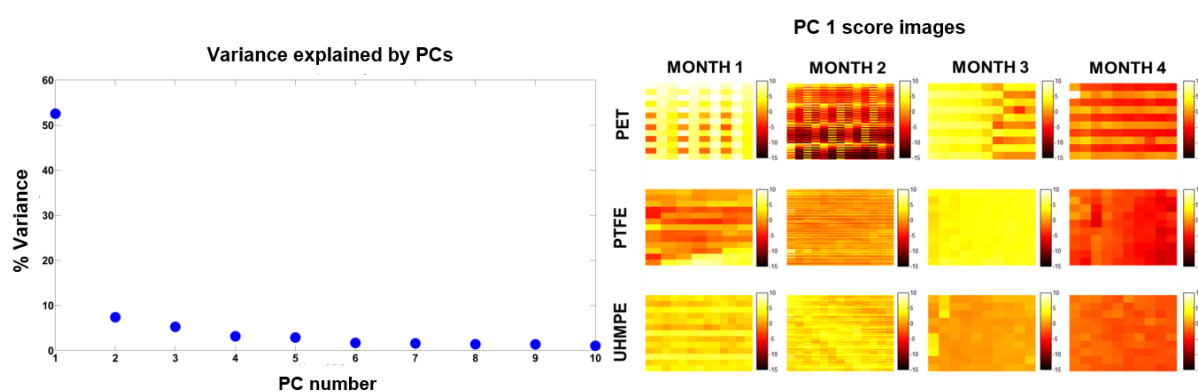
259 (bottom). A lighter pixel colour indicates higher % of transmittance intensity of the wavenumber 3697 cm⁻¹

260 inferring lower hydrophobicity.

261 In **Figure 6**, the intensity of the SNV treated imaging spectra at 3697 cm^{-1} for the bulk polymers
262 over time is shown. Month 1 and Month 2 images show spatial variation occurring due to the
263 noise presented by the array detector. Consistently, PTFE shows darker pixels, indicating a
264 lower intensity of the wavenumber 3697 cm^{-1} at each pixel followed by UHMPE and PET. This
265 can be compared to the contact angle data presented in **Table 2**, where PTFE shows the highest
266 CA values followed by UHMPE and PET in decreasing order of hydrophobicity. A relationship
267 between level of hydration and hydrophobicity has been found at this particular wavenumber,
268 indicating the spectral feature at 3697 cm^{-1} i.e., a univariate analysis with a single wavenumber
269 image, could be used to visualise the interaction between water and a bulk polymer surface.

270 **PCA Results.**

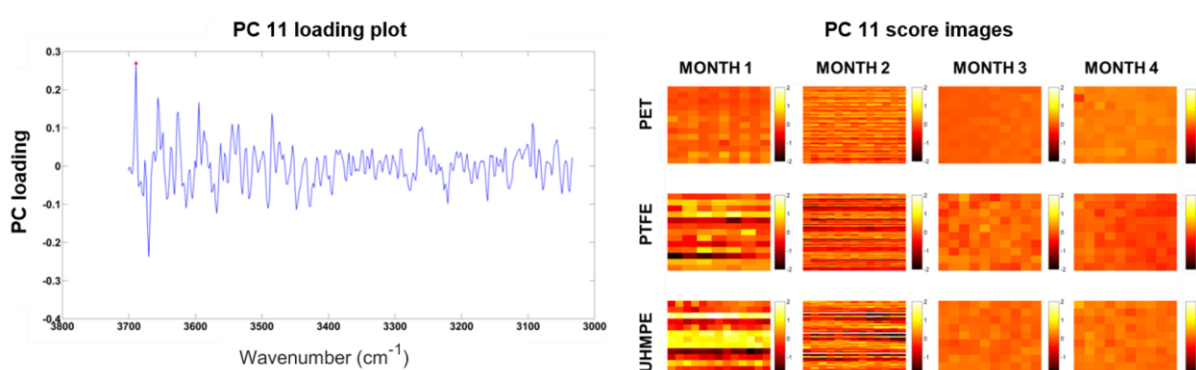
271 The percentage variance accounted for by each PC is plotted in **Figure 7**. PC 1 accounted for
272 52% of the variance. This variation is most likely due to use of the two different detectors, as
273 stated previously. Upon inspection of PC 1 score images (right section, **Figure 7**), the
274 variations due to the detector for Month 1 and month 2 are clearer.



275 **Figure 7.** Variance explained by each PC (left). PC 1 accounts for almost 50% of the variation. Score images for
276 PC 1 are shown in the right, where a lighter pixel colour indicates higher intensity of the PC score.
277

278 To investigate whether there was any correlation between PC scores and CA, the Pearson
279 correlation coefficient was calculated between average PC score (averaged over each image)

280 and CA. PC 11 had the largest absolute correlation coefficient (-0.55, p-value = 0.0040). On
 281 inspecting the loading plot of PC 11 (left section, **Figure 8**), a peak was found at 3690 cm⁻¹
 282 close to the spectral feature 3697 cm⁻¹ discussed previously. The score images for PC 11 for
 283 the bulk polymers are shown in the right section of **Figure 8**. The loading plots and score
 284 images of other PCs were also analysed, but PC 11 showed the highest Pearson correlation
 285 coefficient value. This feature most likely has a similar interpretation to that presented earlier,
 286 the presence of dangling or a disturbed hydrogen bonds due to the interaction of water with the
 287 surfaces of different hydrophobicity.

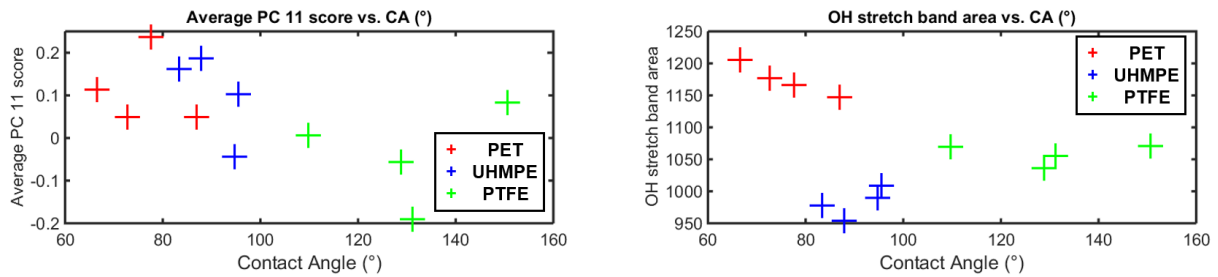


288
 289 **Figure 8.** Loading plot for PC 11 (left) and spatial variation across PC 11 score images (right) for PET (up),
 290 UHMPE (centre) and PTFE (bottom) over time. Lighter colour of the pixel indicates higher intensity of the PC
 291 11 loading prominent feature at wavenumber 3690 cm⁻¹ inferring lower hydrophobicity for PET and UHMPE.

292 With PC 11 score images it is quite difficult to see a consistent pattern or trend visualising the
 293 interaction between water and polymers. Month 4 PC 11 score image for PTFE shows darker
 294 pixels indicating higher hydrophobicity, whereas Month 1 for PTFE score images shows a
 295 higher number of lighter pixels. This might be explained by the fact that; the polymer surfaces
 296 exhibit a heterogeneous nature of hydrophobicity as seen in differences for CA for individual
 297 polymers in **Table 2** which is reflected in the score images in **Figure 8**.

298 A comparison between the use of band area of the OH stretch and the use of PCA to explore
 299 the variation in the OH $\bar{\nu}_S$ region can be visualised in **Figure 9**. The left part of this figure

300 shows the average PC 11 scores for all the polymers over time plotted as a function of contact
301 angle. The right section of the figure shows the relationship between the OH $\bar{\nu}_S$ band area for
302 the bulk polymers over time and the contact angle. While bulk polymers with a high
303 hydrophobicity show a lower value of average PC 11 scores, this trend deviates for UHMPE
304 data when comparing the OH $\bar{\nu}_S$ band area.



305

306 **Figure 9.** Comparison of average PC 11 scores (left) and OH stretch band area (right) as a function of contact
307 angle for PET (red), UHMPE (blue) and PTFE (green) over time.

308 HMDSO coated silicon wafers

309 The CA data for the control and experimental sets of the HMDSO coated silicon wafers are
310 shown in **Table 4** and **Table 5**, which indicate that all the experimental HMDSO coated wafers
311 reach a similar state of hydrophobicity (80-100°) after 5 months. The control sets tended to
312 better maintain their hydrophobic properties, but the hydrophilic coating increased in
313 hydrophobicity after the first month, indicating that precautions such as removal of dust with
314 compressed air, minimising contact with surface must be taken while handling the hydrophilic
315 coated wafer. It is also well established that hydrophilic plasma polymers and plasma treated
316 polymers tend to recover their hydrophobicity over time^{24,25}, and this can also be accelerated
317 due to water diffusion into the interface²⁶. In the case of experimental sets, the protocol used
318 to collect the CA and ATR-FTIR spectra increase the rate of this recovery. Also, repeated
319 handling was likely associated with damage to the nano-structured morphology¹² of the

320 superhydrophobic layers as the ATR crystal exerts pressure on the HMDSO-coated wafers.
 321 **(Table 4).**

322 **Table 4** CA data (Mean value and standard deviation in degrees) for the control set of HMDSO coated silicon
 323 wafers over four months.

	Month 1	Month 2	Month 4	Month 5
Hydrophilic	5 ± 0	47.18 ± 0.07	54.30 ± 1.11	57.85 ± 0.89
Hydrophobic	111.33 ± 0.44	103.1 ± 1.67	111.33 ± 1.65	102.90 ± 2.11
Superhydrophobic	156 ± 0	140.27 ± 0.04	150.32 ± 1.92	148.28 ± 2.60

324

325 **Table 5** CA data (Mean value and standard deviation in degrees) for the experimental set of HMDSO coated
 326 silicon wafers over four months.

	Month 1	Month 2	Month 4	Month 5
Hydrophilic	5 ± 0	53.99 ± 7.95	74.15 ± 5.51	78.63 ± 4.69
Hydrophobic	109 ± 0	100.33 ± 5.33	109.10 ± 1.07	101.54 ± 4.23
Superhydrophobic	174.33 ± 0	100.76 ± 8.93	90.78 ± 4.42	102.42 ± 3.30

327

328 On further examination of the relationship between CA data of the HMDSO coated wafers and
 329 the OH $\bar{\nu}_S$ band area, we found no consistent trend (**Table 6**). Coatings with similar
 330 hydrophobicity have a similar OH $\bar{\nu}_S$ band. This is probably reflective of the similarity of the
 331 hydrophobic coatings over time as indicated by CA data for the experimental HMDSO set in
 332 **Table 5**, which is contributed to by repeated testing on the same sample.

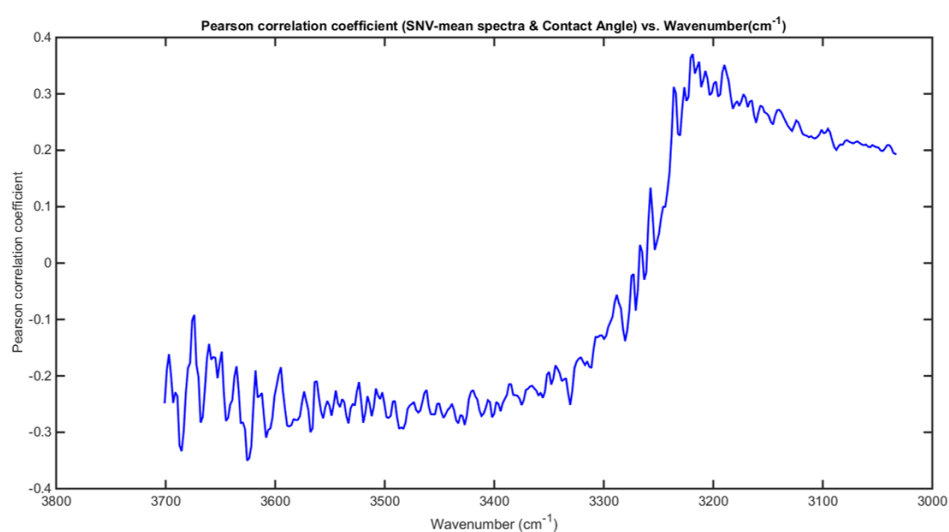
333 **Table 6** Mean and standard deviation of OH $\bar{\nu}_S$ band area data for the experimental set of HMDSO coated
 334 silicon wafers over four months.

	Month 1	Month 2	Month 4	Month 5

Hydrophilic	10329.59 ± 632.22	10422.57 ± 815.25	3205.88 ± 2138.38	10854.34 ± 557.84
Hydrophobic	10880.33 ± 242.88	10629.27 ± 800.20	10492.37 ± 760.58	10092.94 ± 2680.56
Superhydrophobic	9361.6 ± 343.81	12226.82 ± 244.65	9486.79 ± 2134.90	11661.24 ± 443

335

336 The Pearson correlation coefficient between the SNV treated mean spectra for all the HMDSO
 337 treated wafers and mean CA data as a function of wavenumbers in the OH $\bar{\nu}_S$ region is
 338 presented in **Figure 10**.



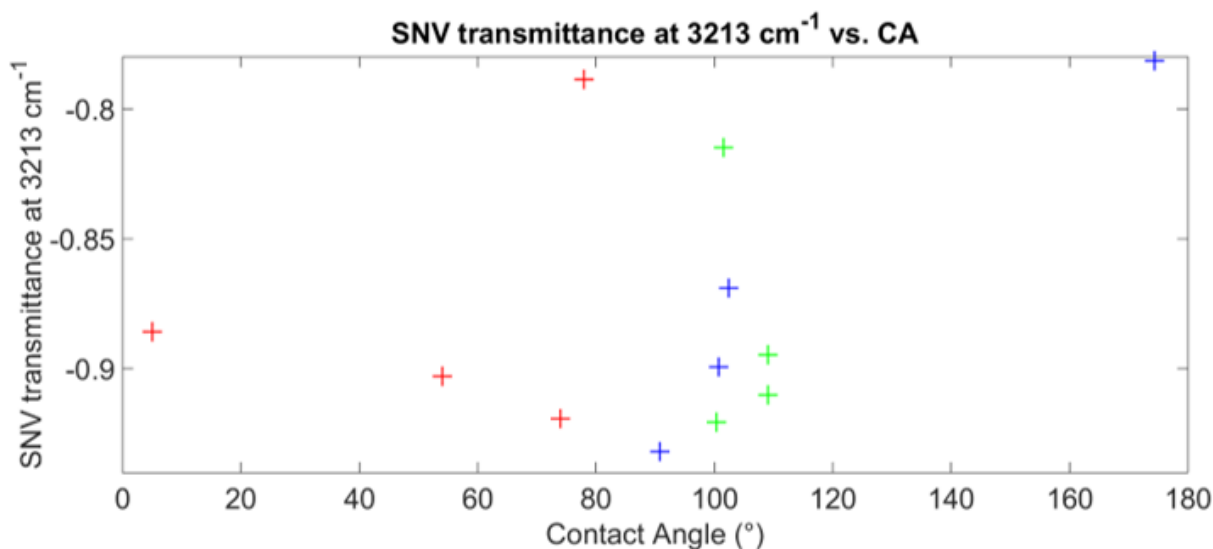
339

340 **Figure 10.** Pearson correlation coefficient calculated between SNV-mean spectra & CA data as a function of
 341 wavenumber (cm^{-1}). Very low correlation observed near 3200 cm^{-1} (0.35)

342 Although we stress that the individual Pearson correlation coefficients were very low, the
 343 highest relative values were observed at 3626 cm^{-1} and near 3200 cm^{-1} ($3216, 3213$ and 3190
 344 cm^{-1}), with a value for each one of $-0.35, 0.37, 0.36$ and 0.35 respectively. A peak at 3220 cm^{-1}
 345 ¹ has previously been reported to be related with hydrogen bond formation between water
 346 molecules on the Raman OH $\bar{\nu}_S$ band ²⁷. Therefore, these weak correlation coefficients could
 347 indicate a relationship between the wavenumbers of the OH $\bar{\nu}_S$ region and the hydrophobicity
 348 of the HMDSO coated silicon wafers. The shift of the band near 3220 cm^{-1} could be due to the
 349 formation of some interaction between the water's hydrogen and the coating. In **Figure 11**, a

350 trend cannot be found between the SNV corrected absorbance at 3200cm^{-1} and CA data for
351 these coatings.

352



353

354 **Figure 11.** SNV transmittance at 3213 cm^{-1} as a function of contact angle data for HMDSO coated Si wafers.
355 (red-hydrophilic, green – hydrophobic, blue – superhydrophobic)

356 According to the calculated OH $\bar{\nu}_S$ areas for HMDSO wafers (Table 6), the value for the
357 hydrophilic wafer at Month 4 appears to be very different when compared to rest of the data.
358 An explanation for this could be that the ATR crystal damaged the spatial region where the
359 data was collected. In order to check whether this particular data point skewed the correlation
360 between CA and the intensity of the SNV treated transmittance for wavenumbers in the OH $\bar{\nu}_S$
361 region, Hydrophilic-Month 4 data was removed from the data matrix and the Pearson
362 correlation coefficient was recalculated. However, an analysis of the modified data matrix did
363 not indicate a possible trend or explanation for this behaviour.

364 As with the bulk polymers, PCA on the SNV treated OH $\bar{\nu}_S$ region of the HMDSO coated
365 silicon wafers was carried out and correlations between the PC scores and the CA data were
366 calculated. A very low correlation (0.4, p-value = 0.2) was found for PC 7 and PC 13 but the

367 p-value indicated that the correlation was not significant. Similarly, removal of hydrophilic-
368 month 4 data showed no improvement in the correlation coefficient between PC scores and CA
369 data.

370 **CONCLUSIONS**

371 The interaction between polymers and water using ATR-FTIR hyperspectral imaging was
372 investigated, focussing on the OH stretching vibration $\bar{\nu}_S$ band region. We compared two
373 categories of polymeric biomaterials, bulk polymers and HMDSO coated silicon wafers. Using
374 contact angle data, we characterised the hydrophobicity of the polymeric biomaterials and
375 investigated the relationship between it and the OH $\bar{\nu}_S$ band region of the mid IR. We found a
376 significant correlation between the CA data of the bulk polymers and ATR-IR spectra at 3697
377 cm^{-1} indicative of the disturbed or disrupted hydrogen bonding networks near such surfaces.
378 Multivariate analysis of bulk polymers was carried out and the band area of the OH $\bar{\nu}_S$ region
379 was also analysed. The results indicated a significant correlation between PC 11 scores and
380 CA, while lower OH $\bar{\nu}_S$ band areas were observed for bulk polymers with a higher degree of
381 hydrophobicity. This indicates that ATR-IR imaging shows potential for studying interactions
382 between bulk polymers and water.

383 However, HMDSO coatings in contact with water did not show a repeatable correlation
384 between CA data and hydrated spectral features acquired through ATR-FTIR imaging, likely
385 due to aging of the coatings and damage to the surface coatings due to repeated testing of the
386 specimens.

387 **ACKNOWLEDGEMENTS**

388 The authors gratefully acknowledge funding from the EU FP7 under the European Research
389 Council Starting Grant programme (ERC-SG-335508). This work was presented as part of
390 IASIM 2016, Chamonix-Mt. Blanc, France.

391 **REFERENCES**

- 392 1. Auras, R., Harte, B. & Selke, S. An overview of polylactides as packaging materials.
393 *Macromol. Biosci.* **4**, 835–864 (2004).
- 394 2. Khandare, J. & Haag, R. Pharmaceutically used polymers: Principles, structures, and
395 applications of pharmaceutical delivery systems. *Handbook of Experimental*
396 *Pharmacology* **197**, 221–250 (2010).
- 397 3. Teo, A. J. T. *et al.* . Polymeric Biomaterials for Medical Implants and Devices. *ACS*
398 *Biomaterial Science and Engineering* **2**, 454–472 (2016).
- 399 4. Bhattacharyya, D., Xu, H., Deshmukh, R. R., Timmons, R. B. & Nguyen, K. T.
400 Surface chemistry and polymer film thickness effects on endothelial cell adhesion and
401 proliferation. *J. Biomed. Mater. Res. A* **94**, 640–8 (2010).
- 402 5. Stallard, C. P., McDonnell, K. a, Onayemi, O. D., O’Gara, J. P. & Dowling, D. P.
403 Evaluation of protein adsorption on atmospheric plasma deposited coatings exhibiting
404 superhydrophilic to superhydrophobic properties. *Biointerphases* **7**, 31 (2012).
- 405 6. Donelli, I., Freddi, G., Nierstrasz, V. A. & Taddei, P. Surface structure and properties
406 of poly-(ethylene terephthalate) hydrolyzed by alkali and cutinase. *Polym. Degrad.*
407 *Stab.* **95**, 1542–1550 (2010).
- 408 7. Tanaka, M., Hayashi, T. & Morita, S. The roles of water molecules at the biointerface
409 of medical polymers. *Polym. J.* **45**, 701–710 (2013).
- 410 8. Chen, S., Li, L., Zhao, C. & Zheng, J. Surface hydration: Principles and applications
411 toward low-fouling/nonfouling biomaterials. *Polymer (Guildf)*. **51**, 5283–5293 (2010).
- 412 9. Chandler, D. Interfaces and the driving force of hydrophobic assembly. *Nature* **437**,
413 640–647 (2005).

- 414 10. Bunkin, N. *et al.* . Study of the Phase States of Water Close to Nafion Interface. *Water*
415 *journal* **4**, 129–154 (2013).
- 416 11. Vogler, E. A. Structure and reactivity of water at biomaterial surfaces. *Adv. Colloid*
417 *Interface Sci.* **74**, 69–117 (1998).
- 418 12. Stallard, C. P., Iqbal, M. M., Turner, M. M. & Dowling, D. P. Investigation of the
419 Formation Mechanism of Aligned Nano-Structured Siloxane Coatings Deposited
420 Using an Atmospheric Plasma Jet. 888–903 (2013).
- 421 13. Kwok, D. Y., Gietzelt, T., Grundke, K., Jacobasch, H.-J. & Neumann, A. W. Contact
422 Angle Measurements and Contact Angle Interpretation. 1. Contact Angle
423 Measurements by Axisymmetric Drop Shape Analysis and a Goniometer Sessile Drop
424 Technique. *Langmuir* **13**, 2880–2894 (1997).
- 425 14. Butt, H.-J. *et al.* . Characterization of super liquid-repellent surfaces. *Curr. Opin.*
426 *Colloid Interface Sci.* **19**, 343–354 (2014).
- 427 15. Socrates, G. *Infrared and Raman characteristic group frequencies. Infrared and*
428 *Raman characteristic group frequencies* (John Wiley & Sons, 2004).
- 429 16. Bellamy, L. J. *The Infrared Spectra of Complex Molecules.* (Chapman and Hall, 1980).
430 doi:10.1007/978-94-011-6520-4
- 431 17. Tassaing, T., Danten, Y. & Besnard, M. Infrared spectroscopic study of hydrogen-
432 bonding in water at high temperature and pressure. *J. Mol. Liq.* **101**, 149–158 (2002).
- 433 18. Esquerre, C., Gowen, A. A., Burger, J., Downey, G. & O'Donnell, C. P. Suppressing
434 sample morphology effects in near infrared spectral imaging using chemometric data
435 pre-treatments. *Chemom. Intell. Lab. Syst.* **117**, 129–137 (2012).
- 436 19. Rodgers, J. L., W. A. N. Thirteen ways to look at the correlation coefficient. *Am. Stat.*

- 437 **42**, 59–66 (1988).
- 438 20. Wold, S., Esbensen, K. & Geladi, P. Principal component analysis. *Chemom. Intell.*
439 *Lab. Syst.* **2**, 37–52 (1987).
- 440 21. Chan, K. L. . & Kazarian, S. . Visualisation of the heterogeneous water sorption in a
441 pharmaceutical formulation under controlled humidity via FT-IR imaging. *Vib.*
442 *Spectrosc.* **35**, 45–49 (2004).
- 443 22. Takeuchi, M., Bertinetti, L., Martra, G., Coluccia, S. & Anpo, M. States of H₂O
444 adsorbed on oxides: An investigation by near and mid infrared spectroscopy. *Appl.*
445 *Catal. A Gen.* **307**, 13–20 (2006).
- 446 23. Binder, H. Water near lipid membranes as seen by infrared spectroscopy. *Eur.*
447 *Biophys. J.* **36**, 265–279 (2007).
- 448 24. Hillborg, H., Tomczak, N., Ola, A., Scho, H. & Vancso, G. J. Nanoscale Hydrophobic
449 Recovery : A Chemical Force Microscopy Study of UV / Ozone-Treated Cross-Linked
450 Poly (dimethylsiloxane). 785–794 (2004).
- 451 25. Hegemann, D., Brunner, H. & Oehr, C. Plasma treatment of polymers for surface and
452 adhesion improvement. *Nucl. Instruments Methods Phys. Res. Sect. B Beam Interact.*
453 *with Mater. Atoms* **208**, 281–286 (2003).
- 454 26. Schäfer, M. M., Seidel, C., Fuchs, H. & Voetz, M. Suppression of water-diffusion in
455 polycarbonate through Ar- and He-plasma as a new model for the origin of improved
456 adhesion of Al. *Appl. Surf. Sci.* **173**, 1–7 (2001).
- 457 27. Sun, Q. Raman spectroscopic study of the effects of dissolved NaCl on water structure.
458 *Vibrational Spectroscopy*, **62**, 110-114 (2012).
- 459